ACS APPLIED MATERIALS & INTERFACES

Research Article

www.acsami.org

Effect of a Long Alkyl Group on Cyclopentadithiophene as a Conjugated Bridge for D−A−π−A Organic Sensitizers: IPCE, Electron Diffusion Length, and Charge Recombination

Qipeng Chai,[†] Wenqin Li,[†,‡] Yongzhen Wu,[†] Kai Pei,[†] Jingchuan Liu,[†] Zhiyuan Geng,[§] He Tian,[†] and Weihong Zhu*[,†]

[†]Shanghai Key Laboratory of Functional Materials Chemistry, Key Laboratory for Advanced Materials and Institute of Fine Chemicals, East China University of Science and Technology, Shanghai 200237, P. R. China

[‡]School of Urban Development and Environmental Engineering, Shanghai Second Polytechnic University, Shanghai 201209, P. R. China

[§]Gansu Key Laboratory of Polymer Materials, College of Chemistry and Chemical Engineering, Key Laboratory of Eco-environment-related Polymer Materials, Ministry of Education, Northwest Normal University, Lanzhou, 730070 Gansu, P. R. China

Supporting Information

ABSTRACT: The option of using conjugated π-linkers is critical for rational molecular design toward an energy-level strategy for organic sensitizers. To further optimize photovoltaic performance, methyl- and octyl-substituted 4*H*-cyclopenta[2,1-*b*:3,4-*b*′]dithiophene (CPDT) are introduced into D−A−π−A featured sensitizers. Along with CPDT, instead of thiophene as conjugated bridge, **WS-39** and **WS-43** exhibit an extended spectral response due to the excellent conjugation and coplanarity of CPDT. Specifically, we focused on the critical effect of length of the alkyl group linked to the bridging carbon atoms of CPDT on the photovoltaic performances. Octyl-substituted **WS-39** shows a broader IPCE onset with an enhanced photovoltage relative to the analogue **WS-5**. In contrast, **WS-43**, with methyl substituted on the CPDT moiety, presents a relatively low quantum conversion efficiency within the whole spectral response region, along with low photocurrent density. **WS-43** displays a distinctly low IPCE platform, predominately arising from the short electron diffusion length with significant electron loss during the electron transport. The relative movement of the conduction band edge (E_{CB}) and charge transfer resistance as well as lifetime of injected electrons are studied in detail. Under standard AM 1.5 conditions, **WS-39**-based solar cells show a promising photovoltaic efficiency of 9.07% (J_{SC} = 16.61 mA cm^{-2}, V_{OC} = 770 mV, FF = 0.71). The octyl chains attached on CPDT can provide *dual protection* and exhibit a high propensity to prevent binding of the iodide−triiodide redox couple, producing an efficient shielding effect to retard the charge recombination and resulting in improvement of V_{OC}. Our research paves the way to explore more efficient sensitizers through ingenious molecular engineering.

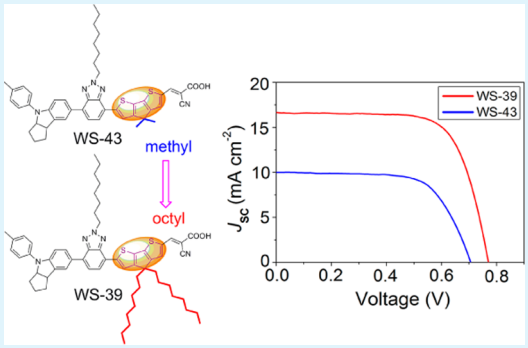

KEYWORDS: *solar cells, organic sensitizers, conjugation bridge, alkyl group, electron diffusion length, photovoltaic efficiency*

INTRODUCTION

Dye-sensitized solar cells (DSSCs) are becoming a promising next-generation alternative to conventional photovoltaic devices due to their high performance price ratio since the innovation by Grätzel and co-workers.[1−6] Ruthenium (Ru) polypyridyl complexes hold the record for overall light to electricity conversion efficiency despite limited noble metal resources and complicated purification procedures.[7−10] Comparatively, metal-free organic sensitizers are of great potential considering their high molar extinction coefficient, tunable molecular structure, and relatively high performance.[11−16] Recently, donor−π−acceptor (D−π−A) featured sensitizers have been intensively developed, especially through delicate molecular modification to affect light harvesting and the band gap between HOMO and LUMO levels.[17−21] Moreover, the incorporation of an auxiliary electron-withdrawing unit between the donor and conjugated bridge can modulate energy level, extend light response, and bring a beneficial electron transfer from the donor to anchor unit, thus efficiently resulting in a great enhancement of both the dye stability and photovoltaic conversion efficiency.[22−36]

Received: June 20, 2014
Accepted: July 25, 2014
Published: July 25, 2014

dx.doi.org/10.1021/am503891q | *ACS Appl. Mater. Interfaces* 2014, 6, 14621−14630

The moderately electron-deficient heterocycle benzotriazole, a highly inexpensive and commercially available chemical material, has been exploited in pure organic sensitizers for DSSCs.[37−39] Previously, benzotriazole-based sensitizer **WS-5** showed a relatively high open voltage (V_{OC}) with a promising power conversion efficiency of 8.02%. However, its moderate photocurrent critically limits the photovoltaic performance because of the essentially narrow absorption band both in solution and on TiO_2 films.[37] Generally, extending the light response can be realized with an incremental change in electron-donating ability or conjugation delocalization, thus maximizing photocurrent generation. The 4*H*-cyclopenta[2,1-*b*:3,4-*b*′]dithiophene (CPDT) unit has been recognized as an efficient building block for organic photovoltaics.[40−42] Its fully rigid coplanar structure along with good electron-donating ability is expected to decrease the HOMO−LUMO band gap and facilitate the intramolecular charge transfer process. Furthermore, long alkyl chains can be feasibly introduced at the bridging carbon atom for the sake of improving solubility and reducing the intermolecular interactions to some extent when adsorbed on TiO_2. With these factors in mind, octyl- and methyl-substituted CPDT were specifically incorporated into the skeleton of indoline-based D−A−π−A sensitizers to construct dyes **WS-39** and **WS-43**, respectively, via simply replacing the conjugated thiophene bridge in the known sensitizer **WS-5** (Figure 1). Our results indicate that the length

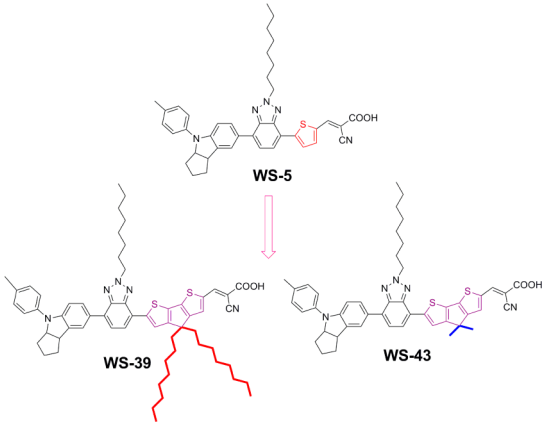

Figure 1. Molecular structures of D−A−π−A sensitizers **WS-39** and **WS-43** derived from reference dye **WS-5**.

of alkyl substituent is crucial to the photovoltaic performance of such CPDT-bridged sensitizers. The two CPDT-based sensitizers **WS-39** and **WS-43** display distinctly different properties on the incident photon-to-current conversion efficiency (IPCE) platform height. In contrast to the IPCE maximum plateaus around 80% in the 400−600 nm region for **WS-5**- and **WS-39**-based cells, there is only 40−50% quantum conversion efficiency for **WS-43** in this region. Along with the electron-diffusion length, the relative movement of the conduction band edge (E_{CB}) and charge transfer resistance as well as lifetime of injected electrons are studied in detail. As demonstrated, the octyl chains attached on CPDT can provide *dual protection*, producing an efficient shielding effect to retard the charge recombination and resulting in improvement of V_{OC}. Under standard AM 1.5 conditions, **WS-39**-based solar cells show a promising photovoltaic efficiency of 9.07% (J_{SC} = 16.61 mA cm^{-2}, V_{OC} = 770 mV, FF = 0.71).

EXPERIMENTAL SECTION

Materials. The starting materials **4**,[37] **1a**,[43] and **1b**[43] were synthesized based on the established literature. Tetrahydrofuran (THF) was dried over and distilled from sodium under argon atmosphere before use. All other chemicals and solvents were purchased as analytical grade and used without further purification.

Instrumentation. The NMR spectra were carried out with a Bruker 400 instrument. High resolution mass spectra (HRMS) were measured with a Waters ESI mass spectrometer. The UV−vis spectra of sensitizers were measured with a model CARY 100 spectrophotometer. Electrochemical measurements were carried out with a three-electrode system, with Pt as working electrode, a saturated calomel reference electrode (SCE) in saturated KCl solution as reference electrode, and a Pt wire as counter electrode. The measurement was performed in CH_2Cl_2 solution, with 0.1 M tetrabutylammonium hexafluorophosphate ($TBAPF_6$) as supporting electrolyte and ferrocene as external standard, and the scan rate was set at 100 mV/s. Electronic impedance spectra (EIS) measurements were performed with an impedance analyzer (Solartron Analytical, 1255B) using DSSC devices under 20 °C in the dark. The magnitude of the sinusoidal perturbations was 5 mV, and the applied frequency range was 10^{-1}−10^5 Hz. The bias potential varied between 550 mV and 650 mV with about 25 mV progressive increase, and the spectra were characterized with Z-View software.

Synthesis. *Synthesis of **2a**.* **1a** (1.0 g, 2.48 mmol) was dissolved in 40 mL of predried THF, the mixture was cooled to −78 °C, a solution of *n*-butyllithium (1.24 mL, 3.0 mmol) was added dropwise under an argon atmosphere, and then anhydrous DMF (0.5 mL, 6.5 mmol) was added after the mixture was stirred under −78 °C for 1 h. Subsequently, the mixture was allowed to react for another 2 h. Then the mixture was poured into water, extracted with CH_2Cl_2 (50 mL × 3), and dried over anhydrous Na_2SO_4. After removal of the solvent, the residue was purified by column chromatography on silica (CH_2Cl_2:petroleum ether = 1:2) to give a pale yellow oil (730 mg, yield 68%). ^{1}H NMR (400 MHz, $CDCl_3$, ppm): δ 9.83 (s, 1H), 7.57 (s, 1H), 7.41 (d, *J* = 5.2 Hz, 1H), 6.99 (d, *J* = 4.8 Hz, 1H), 1.83−1.88 (m, 4H), 1.13−1.27 (m, 20H), 0.83−0.93 (m, 10H). ^{13}C NMR (100 MHz, $CDCl_3$, ppm): δ 182.68, 162.47, 158.10, 147.76, 143.07, 135.53, 130.21, 129.61, 121.84, 53.73, 37.59, 31.77, 29.90, 29.29, 29.20, 24.55, 22.60, 14.09. HRMS (ESI, *m*/*z*): [M + H]$^+$ calcd for $C_{26}H_{39}OS_2$: 431.2442; found: 431.2445.

*Synthesis of **2b**.* **2b** was obtained as a pale green solid in a way similar to that for **2a** (450 mg, yield 65%). ^{1}H NMR (400 MHz, $CDCl_3$, ppm): δ 9.83 (s, 1H), 7.63 (s, 1H), 7.41 (, *J* = 4.8 Hz, 1H), 7.05 (d, *J* = 4.8 Hz, 1H), 1.50 (s, 6H).

*Synthesis of **3a**.* *N*-Bromosuccinimide (NBS, 371.9 mg, 2.09 mmol) was added in portions to a solution of **2a** (600 mg, 1.39 mmol) in THF (40 mL) and stirred for 3 h at room temperature. The reaction mixture was poured into water and extracted with CH_2Cl_2 (50 mL × 3). The organic layer was combined, the solvent was removed by rotary evaporation, and the residue was purified by column chromatography on silica (CH_2Cl_2:petroleum ether = 1:2) to give a pale yellow oil (550 mg, yield 77%). ^{1}H NMR (400 MHz, $CDCl_3$, ppm): δ 9.83 (s, 1H), 7.55 (s, 1H), 7.01 (s, 1H), 1.76−1.89 (m, 4H), 1.13−1.25 (m, 20H), 0.83−0.93 (m, 10H). ^{13}C NMR (100 MHz, $CDCl_3$, ppm): δ 182.94, 161.38, 157.43, 147.09, 143.75, 136.19, 130.24, 125.21, 116.53, 54.87, 37.79, 32.06, 30.16, 29.57, 29.50, 24.81, 22.90, 14.38. HRMS (ESI, *m*/*z*): [M + H]$^+$ calcd for $C_{26}H_{38}BrOS_2$: 509.1547; found: 509.1551.

*Synthesis of **3b**.* **3b** was obtained as a pale green solid in a way similar to that for **3a** (350 mg, yield 63%). ^{1}H NMR (400 MHz, $CDCl_3$, ppm): δ 9.83 (s, 1H), 7.62 (s, 1H), 7.07(s, 1H), 1.48 (s, 6H).

*Synthesis of **5**.* A mixture of **4** (500 mg, 0.90 mmol), bispinacolatodiboron (685.6 mg, 2.7 mmol), KOAc (265.0 mg, 2.7 mmol), and $PdCl_2$(dppf) (40 mg, 0.05 mmol) in anhydrous 1,4-dioxane (25 mL) was stirred at 90 °C for 12 h. The reaction mixture was poured into water and extracted with CH_2Cl_2 (50 mL × 3). The organic layer was collected and dried over Na_2SO_4. After removal of

Scheme 1. Synthetic Route to WS-39 and WS-43

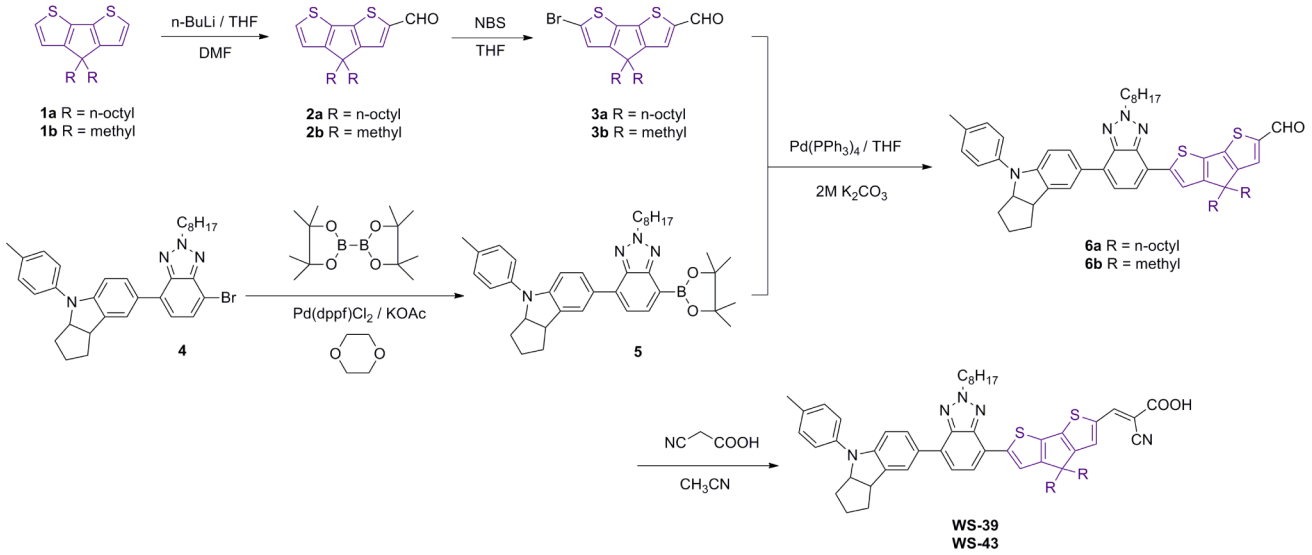

the solvent, the residue was purified by a flash column chromatography on silica (CH_2Cl_2:EtOAc = 20:1) to give a yellow oil.

*Synthesis of **6a***. A mixture of compound **3a** (300 mg, 0.59 mmol), K_2CO_3 (2 M, 10 mL), and $Pd(PPh_3)_4$ (40 mg, 0.03 mmol) were dissolved in THF (30 mL) and heated to reflux under argon atmosphere for 30 min. Compound **5** dissolved in THF (20 mL) was added slowly and refluxed for further 8 h. After cooling to room temperature, the mixture was extracted with CH_2Cl_2 (50 mL × 3). The organic layer was collected and dried over anhydrous Na_2SO_4. After the solvent was evaporated, the residue was purified by column chromatography on silica (CH_2Cl_2:petroleum ether = 1:1) to give a red oil (190 mg, yield 36%). ^{1}H NMR (400 MHz, $CDCl_3$, ppm): δ 9.84 (s, 1H), 7.92 (s, 1H), 7.87 (d, J = 8.4 Hz, 1H), 7.84 (s, 1H), 7.73 (d, J = 7.6 Hz, 1H), 7.58 (s, 1H), 7.52 (d, J = 8.0 Hz, 1H), 7.24 (d, J = 8.4 Hz, 2H), 7.18 (d, J = 8.4 Hz, 2H), 7.04 (d, J = 8.4 Hz, 1H), 4.82–4.88 (m, 3H), 3.93–3.96 (m, 1H), 2.35 (s, 3H), 2.19–2.23 (m, 2H), 2.06–2.10 (m, 1H), 1.93–1.97 (m, 6H), 1.81–1.85 (m, 1H), 1.61–1.70 (m, 2H), 1.16–1.33 (m, 30H), 1.03–1.04 (m, 4H), 0.80–0.89 (m, 9H). ^{13}C NMR (100 MHz, $CDCl_3$, ppm): δ 182.49, 163.38, 157.91, 148.30, 148.25, 145.63, 143.19, 143.07, 142.14, 140.25, 135.43, 135.40, 131.53, 131.20, 130.02, 129.79, 128.26, 127.05, 124.71, 122.83, 122.50, 122.02, 120.30, 120.15, 107.59, 69.23, 56.77, 54.11, 45.48, 37.74, 35.18, 33.77, 31.80, 31.45, 30.11, 30.01, 29.36, 29.26, 29.16, 29.06, 26.68, 24.67, 24.47, 22.65, 22.61, 20.82, 14.11, 14.08. HRMS (ESI, m/z): $[M + H]^+$ calcd for $C_{58}H_{75}N_4OS_2$: 907.5382; found: 907.5383.

*Synthesis of **6b***. **6b** was obtained as a red oil in a way similar to that for **6a** (130 mg, yield 42%). ^{1}H NMR (400 MHz, $CDCl_3$, ppm): δ 9.84 (s, 1H), 8.00 (s, 1H), 7.87 (d, J = 8.4 Hz, 1H), 7.84 (s, 1H), 7.71 (d, J = 7.6 Hz, 1H), 7.64 (s, 1H), 7.52 (d, J = 7.6 Hz, 1H), 7.24 (d, J = 8.0 Hz, 2H), 7.18 (d, J = 8.0 Hz, 2H), 7.03 (d, J = 8.4 Hz, 1H), 4.81–4.88 (m, 3H), 3.92–3.96 (m, 1H), 2.35 (s, 3H), 2.17–2.23 (m, 2H), 2.05–2.12 (m, 1H), 1.95–1.98 (m, 2H), 1.78–1.87 (m, 1H), 1.58 (s, 6H), 1.28–1.43 (m, 12H), 0.85–0.87 (m, 3H). ^{13}C NMR (100 MHz, $CDCl_3$, ppm): δ 182.40, 165.58, 160.40, 148.24, 147.03, 145.98, 143.38, 143.17, 142.12, 140.23, 135.41, 133.98, 131.52, 131.26, 129.78, 129.41, 128.26, 127.00, 124.70, 122.90, 122.49, 121.95, 120.14, 119.83, 107.57, 69.21, 56.76, 45.57, 45.47, 35.17, 33.76, 31.78, 30.14, 29.15, 29.04, 26.66, 25.11, 24.46, 22.64, 20.81, 14.09. HRMS (ESI, m/z): $[M + H]^+$ calcd for $C_{44}H_{47}N_4OS_2$: 711.3191; found: 711.3187.

*Synthesis of **WS-39***. Intermediate **6a** (130 mg, 0.14 mmol) and cyanoacetic acid (119 mg, 1.4 mmol) were dissolved in acetonitrile (20 mL) in the presence of piperidine (0.5 mL) and then refluxed for 8 h under argon atmosphere. The mixture was washed with water and then extracted with CH_2Cl_2 (50 mL × 3), the organic layer was collected and evaporated, and the residue was purified by column chromatography on silica (CH_2Cl_2/MeOH = 10/1) to give a purple black solid (88 mg, yield 63%). ^{1}H NMR (400 MHz, THF-d_8, ppm): δ 8.60 (s, 1H), 8.15 (s, 1H), 7.84–7.92 (m, 3H), 7.66–7.69 (m, 1 H), 7.37–7.60 (m, 1H), 7.16–7.24 (m, 4H), 6.95–6.97 (m, 2H), 4.84–4.88 (m, 3H), 3.86–3.89 (m, 1H), 2.34 (s, 3H), 1.93–2.21 (m, 10H), 1.60–1.68 (m, 2H), 1.22–1.32 (m, 34H), 0.82–0.89 (m, 9H). ^{13}C NMR (100 MHz, THF-d_8, ppm): δ 160.37, 156.51, 145.85, 143.90, 143.04, 141.09, 140.16, 138.56, 135.92, 134.70, 133.99, 133.10, 128.97, 128.61, 127.61, 126.20, 125.38, 122.52, 120.24, 119.98, 118.68, 117.81, 116.58, 105.29, 67.09, 54.44, 52.19, 52.06, 43.53, 35.86, 33.20, 31.72, 29.99, 29.94, 28.26, 28.08, 27.56, 27.50, 27.29, 27.19, 24.74, 20.67, 18.03, 11.64. HRMS (ESI, m/z): $[M - H]^-$ calcd for $C_{61}H_{74}N_5O_2S_2$: 972.5289; found: 972.5286.

*Synthesis of **WS-43***. **WS-43** was obtained as a purple black solid in a way similar to that for **WS-39** (65 mg, yield 72%). ^{1}H NMR (400 MHz, DMSO-d_6, ppm): δ 8.23 (s, 1H), 8.14 (s, 1H), 7.85–7.91 (m, 3H), 7.80 (d, J = 7.6 Hz, 1H), 7.62 (d, J = 7.2 Hz, 1H), 7.23 (d, J = 8.0 Hz, 2H), 7.18 (d, J = 8.0 Hz, 2H), 6.95 (d, J = 8.4 Hz, 1H), 4.84–4.89 (m, 3H), 3.86–3.90 (m, 1H), 2.29 (s, 3H), 2.06–2.08 (m, 2H), 1.77–1.82 (m, 3H), 1.62–1.63 (m, 1H), 1.52 (s, 6H), 1.20–1.33 (m, 12H), 0.78–0.80 (m, 3H). ^{13}C NMR (100 MHz, DMSO-d_6, ppm): δ 164.54, 160.54, 147.34, 144.09, 143.66, 142.17, 141.24, 139.53, 137.40, 135.13, 134.30, 130.72, 129.74, 129.61, 127.92, 126.24, 124.29, 122.58, 122.23, 121.29, 119.75, 119.50, 118.79, 106.92, 68.25, 56.08, 44.93, 44.61, 40.10, 39.89, 39.68, 39.47, 39.26, 39.05, 38.84, 34.83, 33.12, 31.13, 29.25, 28.50, 28.23, 25.90, 24.63, 23.94, 22.02, 20.36, 13.86. HRMS (ESI, m/z): $[M + H]^+$ calcd for $C_{47}H_{48}N_5O_2S_2$: 778.3249; found: 778.3245.

Fabrication of Solar Cells and Photovoltaic Measurements. In the preliminary photovoltaic measurement, we used thin TiO_2 electrodes composed of 6 μm nanoparticles and 4 μm scattering particles. To increase the dye coverage and optimize the overall conversion efficiency, thicker films (9 μm transparent + 4 μm scattering) were utilized. These films were fabricated by repeating the screen printing procedure. The TiO_2 electrodes were sintered at 500 °C for 30 min, followed by treatment with a 40 mM aqueous $TiCl_4$ solution at 70 °C for 30 min and washed with water and ethanol. Afterward, the films were heated again at 500 °C for 30 min and sensitized with dye sensitizer by dipping them into a 3 × 10^{-4} M solution of an optimized binary solvent system ($CHCl_3$:C_2H_5OH = 1:1) for 24 h at room temperature. For preparing the counter electrode, the Pt catalyst was deposited on the cleaned FTO glass by coating with a drop of H_2PtCl_6 solution (0.02 M in 2-propanol solution) with heating at 400 °C for 15 min. A hole (0.8 mm diameter) was predrilled on the counter electrode with a drill press.

Then the counter electrodes were cleaned by ultrasound in an ethanol bath for 10 min.

For the assembly procedure, the dye-covered TiO_2 electrode and Pt counter electrode were assembled into a sandwich type cell and sealed with a hot-melt gasket of 25 μm thickness. A drop of the electrolyte comprising 0.05 M I_2, 0.10 M LiI, 0.60 M DMPII, and 0.50 M 4-TBP in acetonitrile was injected into the cell via vacuum backfilling through the predrilled hole in the counter electrode. Photocurrent density–voltage (I–V) curves were obtained by illuminating the cell through the FTO substrate from the photoanode side under standard AM 1.5 conditions. IPCE measurements were performed on a Newport-74125 system (Newport Instruments).

RESULTS AND DISCUSSION

Design and Synthesis. As demonstrated, the octyl chain in **WS-5** can effectively block I_3^- ions (or iodine) from approaching the TiO_2 surface for charge recombination, thus leading to a strikingly high open voltage.[37] However, **WS-5**-based solar cells exhibit a moderate photocurrent density due to the relatively weak electron-withdrawing capability of the benzotriazole unit. Accordingly, the electron-rich segment (CPDT) was introduced into dye skeleton instead of the traditional thiophene as a conjugated spacer, aiming to optimize the absorption profile and light-harvesting efficiency. As depicted in Scheme 1, two parallel routes were carried out to successfully develop the target molecules. First, the alkyl-substituted CPDT underwent formylation and bromination to afford two crucial intermediates **3a** and **3b**, respectively. The corresponding aldehydes **6a** and **6b** were synthesized through Suzuki reaction between **3a**,**b** and **5**. Finally, the precursors were converted to sensitizers **WS-39** and **WS-43** by typical Knoevenagel condensation with cyanoacetic acid by refluxing in acetonitrile in the presence of piperidine. All the sensitizers were well characterized by ^{1}H and ^{13}C NMR and HRMS. The target molecules can be easily dissolved in common solvents, such as dichloromethane, chloroform, and THF.

Absorption and Electrochemical Properties. The absorption spectra of **WS-39** and **WS-43** and reference dye **WS-5** in CH_2Cl_2 solutions are shown in Figure 2a, and the corresponding properties are summarized in Table 1. The absorption spectra of **WS-5** display three major absorption regions, the maximum absorption peaks can be attributed to intramolecular charge transfer (ICT) from the indoline donor to the anchoring group, and the band around 300 nm is ascribed to the localized aromatic π–π^* transition of the indoline moiety.[44] Furthermore, the peak shoulder of the known sensitizer **WS-5** appears at 393 nm which can facilitate photon capture and conversion. For **WS-39** and **WS-43**, the slight difference in length of the alkyl chain attached to CPDT causes almost identical absorption peaks and molar extinction coefficients. The two developed dyes present a 2-fold difference in molar extinction coefficient on the ICT bands along with an obvious red shift around 20 nm relative to **WS-5**. Such enhanced light-harvesting capability and the bathochromic shift may be ascribed to the electron-rich property and excellent coplanarity of the CPDT bridge, which benefits the capture of photons in an extended region.[44]

Figure 2b shows the absorption spectra of the organic sensitizers anchored onto a 3 μm transparent nanocrystalline TiO_2 film for 20 min. When anchored onto TiO_2 films, the sensitizers may bring forth interactions among dye molecules or between a dye molecule and a nanoparticle of TiO_2. Thus, the absorption spectra of sensitizer adsorbed on TiO_2 are changed to some extent. The absorption peaks of **WS-5**, **WS-39**, and

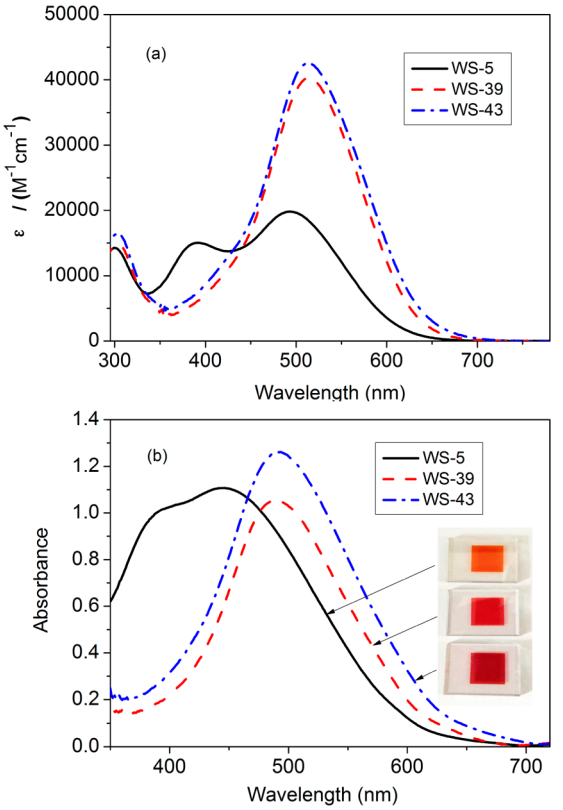

Figure 2. Absorption spectra of **WS-39**, **WS-43**, and reference dye **WS-5**: (a) in CH_2Cl_2, (b) adsorbed onto TiO_2 films for 20 min (3 μm in thickness).

Table 1. Photophysical and Electrochemical Properties of Sensitizers WS-39, WS-43, and Reference Dye WS-5 in CH_2Cl_2 and on TiO_2 Films (3 μm in thickness)

	WS-5	WS-39	WS-43
λ_{max},[a] nm (ε,[a] M^{-1} cm^{-1})	494 (19800) 393 (15000) 300 (14300)	514 (40300) 303 (14900)	514 (42600) 303 (16600)
λ_{max} on TiO_2, nm	446	490	491
HOMO,[c] V	0.85	0.74	0.76
E_{0-0},[d] eV	2.06	2.02	1.97
LUMO,[d] V	−1.21	−1.28	−1.21

[a]Absorption peaks (λ_{max}) and molar extinction coefficients (ε) in CH_2Cl_2 solution. [b]Absorption peaks on 3 μm TiO_2 films. [c]HOMO levels were measured in acetonitrile solution, calibrated with ferrocene/ferrocenium (F_c/F_c^+) as an external reference. [d]E_{0-0} was estimated from the absorption thresholds from absorption spectra of dyes adsorbed on the TiO_2 film. LUMO is estimated by subtracting E_{0-0} from the HOMO.

WS-43 were hypsochromically shifted, which results from deprotonation or H-aggregation. Note that the absorption intensity of **WS-5** is comparable with that of **WS-39** and **WS-43** in a 20 min adsorption, which may be ascribed to more dye molecule uptake in view of its inferior light-harvesting capability. Obviously, **WS-43** adsorbed on TiO_2 film became darker in color than **WS-39** adsorbed on TiO_2 film (Figure 2b). Actually, the absorbance maximum for **WS-43** is 1.2-fold that of **WS-39**, which might result from high dye molecule uptake of **WS-43** having a short alkyl chain on the CPDT unit.

Cyclic voltammetry was carried out to measure the oxidation potentials of the sensitizers and evaluate the thermodynamic

dx.doi.org/10.1021/am503891q | ACS Appl. Mater. Interfaces 2014, 6, 14621–14630

driving force of dye regeneration. As depicted in Figure S1 in Supporting Information (SI), the HOMO levels corresponding to the formal oxidation potentials of the three sensitizers are 0.85, 0.74, and 0.76 V, respectively, which are more positive than that of I_3^-/I^-, indicating a thermodynamic regeneration of the sensitizers. An uplift of the HOMO level by about 0.1 V for **WS-39** and **WS-43** stems from a more electron-rich and large conjugation property for CPDT compared with that for the thiophene moiety. Band gaps (E_{0-0}) for each sensitizer, estimated from the 10% absorption on dye-covered TiO_2 films, are 2.06, 2.02, and 1.97 eV, respectively. Accordingly, the calculated LUMO levels are more negative than the Fermi level of TiO_2 (−0.5 V vs NHE), which ensures a sufficient driving force for electron injection.[45]

Moreover, we used the hybrid B3LYP functional and the standard 6-31G(d) basis set to optimize the ground-state geometries of the sensitizers in the gas phase by DFT with the Gaussian09 package.[46,47] As presented in Figure S2 and Table S1 in SI, the dihedral angles between the electron donor indoline and auxiliary electron-withdrawing benzotriazole have negligible differences among **WS-5** and the other two CPDT-based sensitizers. For the conjugated bridge and the benzotriazole part, the dihedral angles in **WS-5**, **WS-39**, and **WS-43** are 5.5°, 9.3°, and 0.1°, respectively. Obviously, the highly conjugated backbone may be beneficial to the electron injection process. Both of the HOMO orbitals of **WS-39** and **WS-43** are distributed along the D−A−π part, while the LUMOs are delocalized across the A−π−A segment (Figure 3).

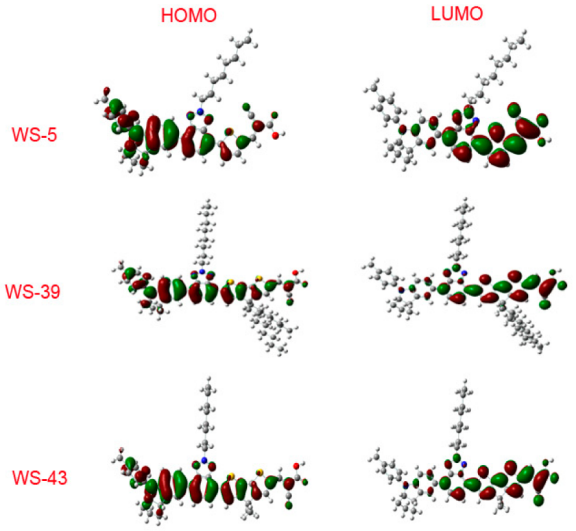

Figure 3. Calculated frontier orbitals of sensitizers **WS-5**, **WS-39**, and **WS-43**.

In the frontier molecular orbitals, the overlap of the electron cloud is located at the auxiliary electron-withdrawing benzotriazole, which may facilitate electron transfer from the indoline donor to the anchor after photoexcitation.[37]

IPCE and Electron Diffusion Length. Along with a better conjugated backbone, sensitizer **WS-39** is beneficial to the harvest of photons from longer wavelength, which is expected to present an extended IPCE response with respect to analogue **WS-5** (Figure 4). Notably, **WS-39** exhibited recessed regions around 400 nm for CPDT-based solar cells, consistent with the spectral responses (Figure 2). Meanwhile, the two CPDT-based sensitizers of **WS-39** and **WS-43** display distinctly different

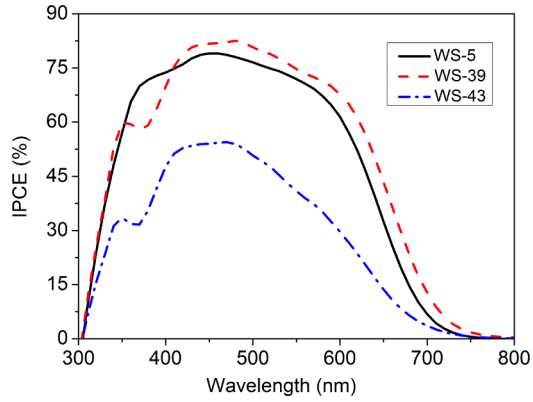

Figure 4. IPCE action spectra of DSSCs based on sensitizers **WS-5**, **WS-39**, and **WS-43** (TiO_2 films: 9 μm transparent + 4 μm scattering nanoparticles).

properties of IPCE platform height. In contrast to the IPCE maximum plateaus around 80% over the range 400−600 nm for **WS-5** and **WS-39**-based cells, there is only 40−50% quantum conversion efficiency for **WS-43** in this region.

To better understand the differences between IPCE plateaus for the three sensitizers, we should carefully analyze the key factors for IPCE. It is well-known that the IPCE of a device is determined by light-harvesting efficiency (LHE), electron injection efficiency (Φ_{inj}), and the electron collection efficiency (Φ_{col}).[48] In view of the almost identical light capture capability of **WS-43** relative to **WS-39** (Figure 2a), LHE is not the determinant for inefficient quantum conversion. Moreover, the similar LUMO levels and the identical anchoring group of the three sensitizers indicate that Φ_{inj} is also not the main cause. Therefore, we expect that low Φ_{col} may lead to the disappointing IPCE plateau and photocurrent of **WS-43**.

In an assembled device, the transport of the injected electrons through the mesoporous TiO_2 nanoparticles to the FTO substrate generates the photocurrent, and the procedure is dominated by diffusion.[49,50] Measurement of the electron diffusion length (L_n, defined as the mean diffusion distance before electron recombination) is always used to evaluate Φ_{col}.[51−53] O'Regan's group has proposed and certified that Φ_{col} could also be assessed by electron collection length L_{col}.[50,51] We can measure L_{col} by testing the wavelength-dependent ratio ($r_{(EE/PE)}$) of photocurrents when illuminating from the electrolyte−electrode side (EE) versus photoanode side (PE).[48,50] The IPCE spectra of the three dyes illuminated from the PE side are depicted in Figure S3 in SI. When L_{col} is longer than the thickness of the photoanode, most photoelectrons are collected and converted to the photocurrent whether the illumination is from back or front, and the $r_{(EE/PE)}$ reaches the maximum. Considering the optical losses on the deposited platinum and the electrolyte in the case of EE illumination, the $r_{(EE/PE)}$ cannot reach unity. If L_{col} is shorter than the thickness of the electrode, the photoelectrons far from the collection electrode are recombined, while the electrons adjacent to the collection electrode will not be influenced. Thus, the value of $r_{(EE/PE)}$ has an obvious drop when the thickness of the film exceeds L_{col}. Figure 5 depicts the plots of $r_{(EE/PE)}$ as a function of thickness, which derives from the IPCE curves when illuminating from the EE side and the PE side. The $r_{(EE/PE)}$ values of **WS-5** and **WS-39** are fundamentally unchanged with the increase in photoelectrode thickness, indicating that L_{col} of both **WS-5** and **WS-39** exceeds 15 μm

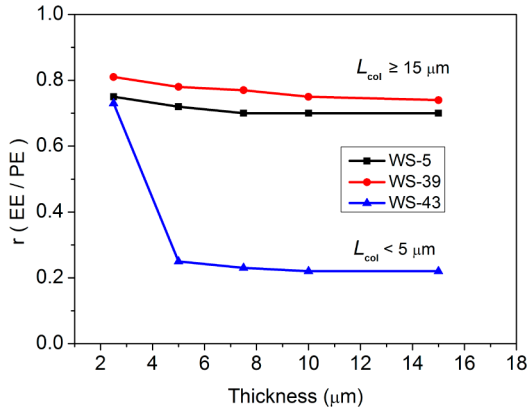

Figure 5. Ratios of photocurrent density derived from the EE side and PE side as a function of TiO_2 electrode thickness sensitized with **WS-5**, **WS-39**, and **WS-43**.

whereas $r_{(EE/PE)}$ of **WS-43** drops dramatically when the thickness of the film increases to 5 μm, meaning that L_{col} of **WS-43** is shorter than 5 μm. Therefore, significant electron loss during electron transport results in the unsatisfactory IPCE plateau of **WS-43** (Figure 5). The systematic photovoltaic performance under this condition is listed in Table 2 for a systematic comparison. **WS-43** exhibited higher photovoltaic efficiency at less thickness (5.23%, 2.5 μm) than at more thickness (4.48%, 6 + 4 μm).

Table 2. Photovoltaic Parameters of DSSCs Measured under AM 1.5 Conditions

TiO_2 electrode	dyes	J_{sc} (mA cm^{-2})	V_{oc} (mV)	FF	η
2.5 μm	**WS-5**	11.68	797	0.66	6.13
	WS-39	13.71	795	0.68	7.42
	WS-43	11.38	730	0.63	5.23
6 + 4 μm	**WS-5**	14.69	765	0.69	7.74
	WS-39	15.05	779	0.69	8.11
	WS-43	9.49	716	0.66	4.48
9 + 4 μm	**WS-5**	15.89	747	0.69	8.19
	WS-39	16.61	770	0.71	9.07
	WS-43	10.03	705	0.67	4.74
9 + 4 μm	**WS-43**[a] (5 mM CDCA)	11.25	714	0.65	5.22

[a]**WS-43** was coadsorbed with 5 mM CDCA.

The $I-V$ characteristics achieved for solar cell devices are illustrated in Figure 6, and the corresponding data are collected in Table 2. In a preliminary photovoltaic test, we chose relatively thin films (6 + 4 μm) sensitized with **WS-5**, **WS-39**, and **WS-43**. The developed sensitizer **WS-39** showed an increased photocurrent density and enhanced open voltage relative to the reference dye **WS-5**. To increase the dye loading amount and optimize the overall conversion efficiency, we further used the thicker TiO_2 electrodes (9 + 4 μm). Also, the photocurrent density of **WS-39** (16.61 mA cm^{-2}) is more promising than that of **WS-5** (15.89 mA cm^{-2}) due to the extended IPCE response under this condition. Under optimized conditions, the **WS-39**-based solar cells achieve a power conversion efficiency up to 9.07% (J_{SC} = 16.61 mA cm^{-2}, V_{OC} = 770 mV, FF = 0.71). However, in contrast with **WS-39**, the power conversion of **WS-43** decreased by 48% to 4.74%. Strangely, here the different alkyl group substitution on the

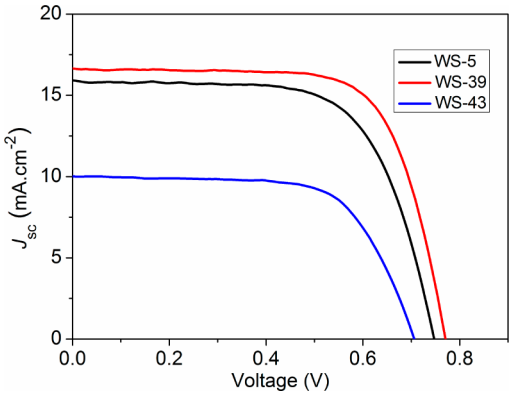

Figure 6. Current–voltage characteristics of **WS-5**, **WS-39**, and **WS-43** (TiO_2 films: 9 μm transparent + 4 μm scattering nanoparticles).

CPDT results in a sharp drop in both J_{SC} and V_{OC}. As mentioned above, the drop in J_{SC} for **WS-43** can be reasonably attributed to the short electron diffusion length with significant electron loss during the electron transport (Figure 5), resulting in much lower J_{SC} and power conversion efficiency.

Conduction Band Movement and Charge Recombination. To gain insight into the intriguing difference (Table 2) in V_{OC} value for **WS-5** (747 mV), **WS-39** (770 mV), and **WS-43** (705 mV) at the thicker TiO_2 films (9 μm transparent + 4 μm scattering), electrochemical impedance spectroscopy (EIS) was performed. Generally, V_{OC} is defined as the potential difference between the Fermi level of TiO_2 (E_{Fn}) and the redox species (E_{red}) in the electrolyte.[54,55] Because the redox potential is kept constant due to the same redox couples used in the experiment, V_{OC} is determined by the position of the TiO_2 conduction band and the electron density in the semiconductor.[56−59] Here we exploited the fitted capacitive response of the cell (C_μ) under a series bias potential to investigate the impact on the position of the TiO_2 conduction band. As shown in Figure 7a, at a given applied potential, the capacitance (C_μ) was decreased in the sequence of **WS-43** > **WS-5** > **WS-39**, indicating a sequential upward trend for E_{CB}.[60−62] The result was in exact accordance with the sequence of V_{OC} values. That is, the variation of V_{OC} is relevant to the change in E_{CB}, which might result from the change in energy levels of the sensitizers upon the adsorption process.[63] Generally, the dipole moments along the direction from sensitizers to TiO_2 (vertical) upon dye adsorption can induce a conduction band shift. Differential sensitizers may have some difference in dipole moment upon dye adsorption.

The interface charge transfer resistance (R_{CT}) and electron lifetime (τ) were also characterized. As shown in Figure 7b, the interface charge transfer resistance was in the order of **WS-39** > **WS-5** > **WS-43**. Especially, under 0.65 V bias potential, the interface charge transfer resistance for **WS-39**-based solar cells was 6-fold that for **WS-43**. Obviously, **WS-39** can suppress charge recombination much more efficiently than **WS-43**, resulting in the highest V_{OC} among the three dyes. Moreover, the calculated electron lifetimes are in the order **WS-39** > **WS-5** > **WS-43** (Figure 7c), which is consistent with the sequence of V_{OC}. Obviously, the concerted contribution from both the interface charge transfer resistance and electron lifetime determines the remarkable difference in V_{OC} values for the three sensitizers.

Correlation between Charge Recombination Rate and Chemical Structure of Sensitizers. As illustrated in Figure

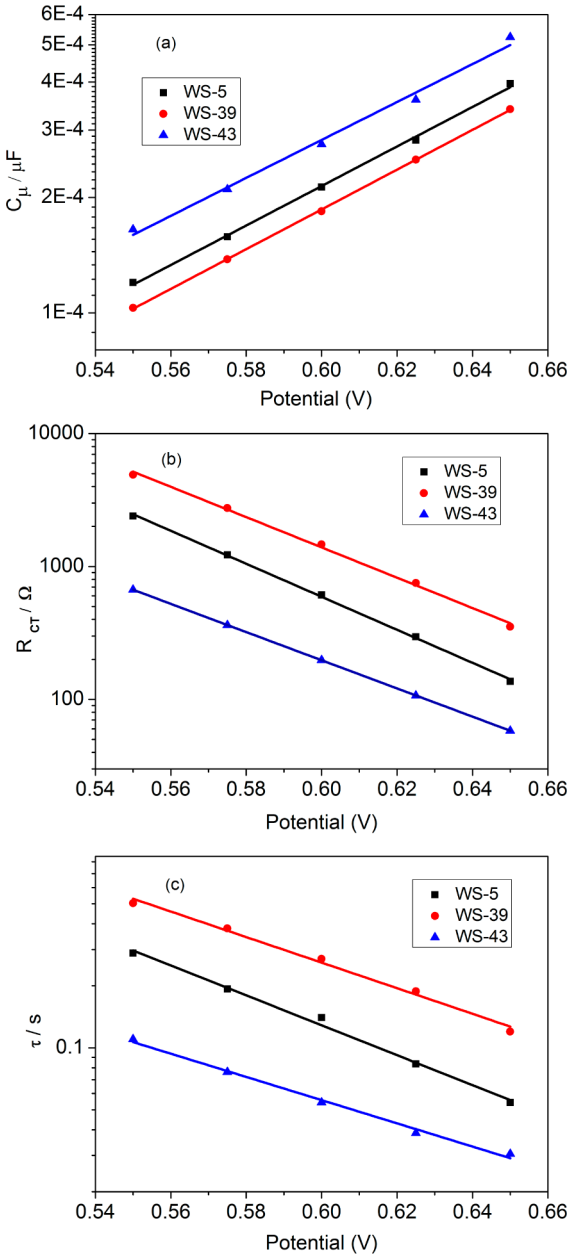

Figure 7. Plots of capacitance (C_μ, a), interface charge transfer resistance (R_{CT}, b), and calculated electron lifetime (τ, c) under a series potential bias of DSSCs based on **WS-5**, **WS-39**, and **WS-43**.

7b, the charge transfer resistances of DSSCs increased in the order of **WS-43** < **WS-5** < **WS-39**, while the charge recombination rate decreased inversely. Generally, the effective blocking and compact pattern of sensitizers adsorbed on TiO_2 are decisive for the improvement in V_{OC}. Accordingly, we can gain further interpretation for the notable difference in V_{OC} values of the sensitizers from the perspective of intrinsic structures. Figure 8 shows the optimized molecular structures of the sensitizers derived from DFT calculations. The heights between the nitrogen atoms of benzotriazole and the TiO_2 surface were calculated. The distance between the 2 position N atom of benzotriazole in **WS-5** and the surface of TiO_2 is 8.92 Å (Figure 8) while for **WS-39** and **WS-43**, the corresponding values were increased to 11.29 and 10.00 Å, respectively. Moreover, the height of the bridged carbon atom in CPDT of **WS-39** is 8.02 Å, which is even below the 2 position N atom of

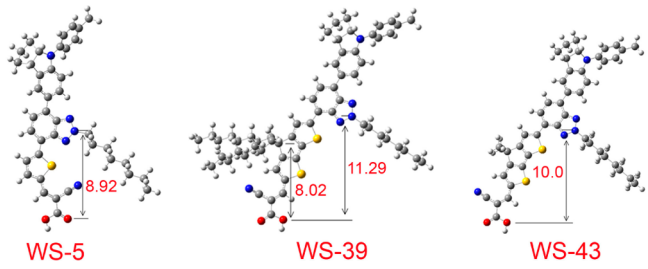

Figure 8. Simulated molecular adsorption tendency onto TiO_2 for sensitizers **WS-5**, **WS-39**, and **WS-43**.

benzotriazole in **WS-5**. Thus, in the case of **WS-39**, the two octyl chains in CPDT may provide effective blocking to suppress the recombination of injected electrons and electron-accepting species.

The adsorption amount was further measured to shed light on possible interactions. The adsorption amount for **WS-43** is 6.25×10^{-8} mol cm^{-2}, which is comparable to that of **WS-5** (6.46×10^{-8} mol cm^{-2})-based solar cells. With respect to **WS-5**, the extended conjugation bridge for **WS-43** leads to more void space between the electrolyte and TiO_2 films, which may facilitate the recombination of injected electrons and redox species. However, for **WS-39**, with an adsorption amount of only 70% (4.42×10^{-8} mol cm^{-2}) that of **WS-43**, the octyl chains attached to the carbon atoms in CPDT moieties are expected to provide another protected area. We also rule out the possibility that the higher adsorption amount of **WS-43** leads to a relatively lower performance. In fact, even upon coadsorption with CDCA (5 mM), the photovoltaic efficiency was only 5.22% (Table 2), still very inferior to that of **WS-39**. We consider, in **WS-39**, that the two types of alkyl chains on CPDT and benzotriazole can comprise a so-called *dual protection* and have a high propensity to prevent binding of the iodide−triiodide redox couple[64] (Figure 9), which may form a compact layer to effectively retard the charge recombination process and also improve the open circuit voltage in the order of **WS-43** (705 mV) < **WS-5** (747 mV) < **WS-39** (770 mV).

CONCLUSIONS

We incorporated alkyl-substituted CPDT into benzotrizole-containing dyes **WS-39** and **WS-43** for exploring more efficient sensitizers through ingenious molecular engineering. The incorporation of CPDT significantly red-shifts the spectral response with respect to thiophene-bridged **WS-5**. We specifically focused on the critical effect of the length of the alkyl group linked to the bridging carbon atoms of CPDT on the photovoltaic performances. Octyl-substituted **WS-39** achieves a promising overall conversion efficiency of 9.07% (J_{SC} = 16.61 mA cm^{-2}, V_{OC} = 770 mV, FF = 0.71), with an enhanced photocurrent and photovoltage relative to **WS-5** whereas the methyl-substituted sensitizer **WS-43** results in quite a disappointing decrease in photovoltaic efficiency to 4.74% (J_{SC} = 10.03 mA cm^{-2}, V_{OC} = 705 mV, FF = 0.67). As demonstrated, the two CPDT-based sensitizers **WS-39** and **WS-43** display distinctly different properties for IPCE platform height. Due to the short electron diffusion length, significant electron loss during electron transport results in an unsatisfactory IPCE plateau for **WS-43**. The octyl chains attached to the CPDT unit of **WS-39** benefit the electron diffusion and transport through the interconnected TiO_2

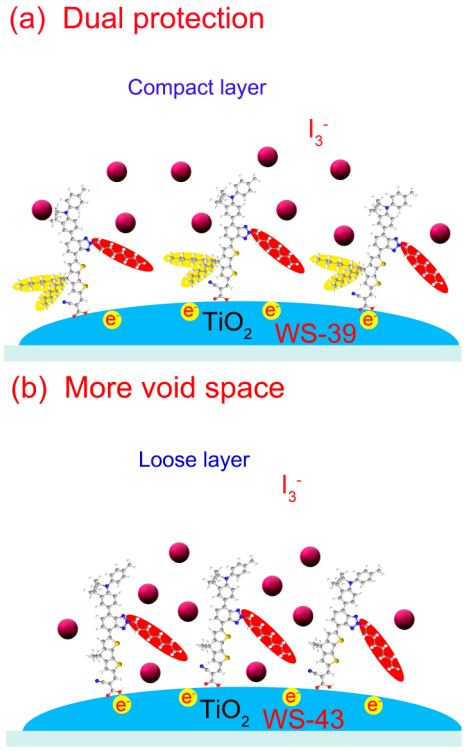

Figure 9. Simulated adsorption models for sensitizers **WS-39** (a) and **WS-43** (b).

particles for maximal photocurrent generation. Moreover, an uplift of the conduction band edge, a relative large charge transfer resistance, and a longer lifetime for the injected electrons result in a higher voltage for **WS-39**-based solar cells. The octyl chains on CPDT provide *dual protection*, producing an efficient shielding effect to retard the charge recombination and resulting in improvement of V_{OC}. This work sets a direction for a rational molecular strategy to achieve high power conversion efficiency, especially to increase light absorption and J_{SC} while avoiding any trade-off by decreasing V_{OC}.

■ ASSOCIATED CONTENT

Supporting Information

Cyclic voltammograms, optimized ground-state geometries, IPCE spectra for different thicknesses, and ^{1}H NMR, ^{13}C NMR and HRMS spectra of sensitizers. This material is available free of charge via the Internet at http://pubs.acs.org.

■ AUTHOR INFORMATION

Corresponding Author

*Fax: (+86) 21-6425-2758. E-mail: whzhu@ecust.edu.cn.

Notes

The authors declare no competing financial interest.

■ ACKNOWLEDGMENTS

This work was supported by the National 973 Program (2013CB733 700), NSFC for Distinguished Young Scholars (grant no. 21325625), NSFC/China, Oriental Scholarship, National Major Scientific Technological Special Project (2012YQ15008709), SRFDP 20120074110002, Fundamental Research Funds for the Central Universities (WK1013002), and Key Discipline Construction (Materials Science, XXKPY1302).

■ REFERENCES

(1) O'Regan, B.; Grätzel, M. A Low-Cost, High-Efficiency Solar Cell Based on Dye-Sensitized Colloidal TiO_2 Films. *Nature* **1991**, *353*, 737−740.
(2) Hagfeldt, A.; Boschloo, G.; Sun, L.; Kloo, L.; Pettersson, H. Dye-Sensitized Solar Cells. *Chem. Rev.* **2010**, *110*, 6595−6663.
(3) Zhang, S.; Yang, X.; Numata, Y.; Han, L. Highly Efficient Dye-Sensitized Solar Cells: Progress and Future Challenges. *Energy Environ. Sci.* **2013**, *6*, 1443−1464.
(4) Fang, Z.; Eshbaugh, A. A.; Schanze, K. S. Low-Bandgap Donor−Acceptor Conjugated Polymer Sensitizers for Dye-Sensitized Solar Cells. *J. Am. Chem. Soc.* **2011**, *133*, 3063−3069.
(5) Hart, A. S.; KC, C. B.; Gobeze, H. B.; Sequeira, L. R.; D'Souza, F. Porphyrin-Sensitized Solar Cells: Effect of Carboxyl Anchor Group Orientation on the Cell Performance. *ACS Appl. Mater. Interfaces* **2013**, *5*, 5314−5323.
(6) Berhe, S. A.; Gobeze, H. B.; Pokharel, S. D.; Park, E.; Youngblood, W. J. Solid-State Photogalvanic Dye-Sensitized Solar Cells. *ACS Appl. Mater. Interfaces* **2014**, *6*, 10696−10705.
(7) Nazeeruddin, M. K.; Kay, A.; Rodicio, I.; Humphry-Baker, R.; Müller, E.; Liska, P.; Vlachopoulos, N.; Grätzel, M. Conversion of Light to Electricity by cis-X_2bis(2,2′-bipyridyl-4,4′-dicarboxylate)-ruthenium(II) Charge-Transfer Sensitizers (X = Cl^-, Br^-, I^-, CN^-, and SCN^-) on Nanocrystalline Titanium Dioxide Electrodes. *J. Am. Chem. Soc.* **1993**, *115*, 6382−6390.
(8) Nazeeruddin, M. K.; Péchy, P.; Grätzel, M. Efficient Panchromatic Sensitization of Nanocrystalline TiO_2 Films by a Black Dye Based on Atrithiocyanato−Ruthenium Complex. *Chem. Commun.* **1997**, 1705−1706.
(9) Han, L.; Islam, A.; Chen, H.; Malapaka, C.; Chiranjeevi, B.; Zhang, S.; Yang, X.; Yanagida, M. High-Efficiency Dye-Sensitized Solar Cell with a Novel Co-Adsorbent. *Energy Environ. Sci.* **2012**, *5*, 6057−6060.
(10) Chou, C. C.; Hu, F. C.; Yeh, H. H.; Wu, H. P.; Chi, Y.; Clifford, J. N.; Palomares, E.; Liu, S. H.; Chou, P. T.; Lee, G. H. Highly Efficient Dye-Sensitized Solar Cells Based on Panchromatic Ruthenium Sensitizers with Quinolinylbipyridine Anchors. *Angew. Chem., Int. Ed.* **2014**, *53*, 178−183.
(11) Yen, Y.-S.; Chou, H.-H.; Chen, Y.-C.; Hsu, C.-Y.; Lin, J. T. Recent Developments in Molecule-Based Organic Materials for Dye-Sensitized Solar Cells. *J. Mater. Chem.* **2012**, *22*, 8734−8747.
(12) Li, G.; Liang, M.; Wang, H.; Sun, Z.; Wang, L.; Wang, Z. H.; Xue, S. Significant Enhancement of Open-Circuit Voltage in Indoline-Based Dye-Sensitized Solar Cells via Retarding Charge Recombination. *Chem. Mater.* **2013**, *25*, 1713−1722.
(13) Zeng, W. D.; Cao, Y. M.; Bai, Y.; Wang, Y. H.; Shi, Y. H.; Zhang, M.; Wang, F. F.; Pan, C. Y.; Wang, P. Efficient Dye-Sensitized Solar Cells with an Organic Photosensitizer Featuring Orderly Conjugated Ethylenedioxythiophene and Dithienosilole Blocks. *Chem. Mater.* **2010**, *22*, 1915−1925.
(14) Zhang, M.; Wang, Y. L.; Xu, M. F.; Ma, W. T.; Li, R. Z.; Wang, P. Design of High-Efficiency Organic Dyes for Titania Solar Cells Based on the Chromophoric Core of Cyclopentadithiophene-Benzothiadiazole. *Energy Environ. Sci.* **2013**, *6*, 2944−2949.
(15) Wu, Y. Z.; Marszalek, M.; Zakeeruddin, S. M.; Zhang, Q.; Tian, H.; Grätzel, M.; Zhu, W. H. High-Conversion-Efficiency Organic Dye-Sensitized Solar Cells: Molecular Engineering on D−A−π−A Featured Organic Indoline Dyes. *Energy Environ. Sci.* **2012**, *5*, 8261−8272.
(16) Mathew, S.; Yella, A.; Gao, P.; Humphrey-Baker, R.; Curchod, B. F. E.; Ashari-Astani, N.; Tavernelli, I.; Rothlisberger, U.; Nazeeruddin, M. K.; Grätzel, M. Dye-Sensitized Solar Cells with 13% Efficiency Achieved through the Molecular Engineering of Porphyrin Sensitizers. *Nat. Chem.* **2014**, *6*, 242−247.
(17) Nguyen, W. H.; Bailie, C. D.; Burschka, J.; Moehl, T.; Grätzel, M.; McGehee, M. D.; Sellinger, A. Molecular Engineering of Organic Dyes for Improved Recombination Lifetime in Solid-State Dye-Sensitized Solar Cells. *Chem. Mater.* **2013**, *25*, 1519−1525.
(18) Grimm, B.; Risko, C.; Azoulay, J. D.; Bredas, J. L.; Bazan, G. C. Molecular Engineering of Organic Dyes for Improved Recombination

Lifetime in Solid-State Dye-Sensitized Solar Cells. *Chem. Sci.* **2013**, *4*, 1807−1819.
(19) Jiang, S. H.; Lu, X. F.; Zhou, G.; Wang, Z.-S. Charge Transfer in Cross Conjugated 4,8-Dithienylbenzo[1,2-*b*:4,5-*b*′]dithiophene Based Organic Sensitizers. *Chem. Commun.* **2013**, *49*, 3899−3901.
(20) Qu, S. Y.; Hua, J. L.; Tian, H. New D-π-A Dyes for Efficient Dye-Sensitized Solar Cells. *Sci. China Chem.* **2012**, *55*, 677−697.
(21) Li, H.; Hou, Y.; Yang, Y.; Tang, R.; Chen, J.; Wang, H.; Han, H.; Peng, T.; Li, Q.; Li, Z. Attempt to Improve the Performance of Pyrrole-Containing Dyes in Dye Sensitized Solar Cells by Adjusting Isolation Groups. *ACS Appl. Mater. Interfaces* **2013**, *5*, 12469−12477.
(22) Zhu, W. H.; Wu, Y. Z.; Wang, S. T.; Li, W. Q.; Li, X.; Chen, J.; Wang, Z.-S.; Tian, H. Organic D-A-π-A Solar Cell Sensitizers with Improving Stability and Spectral Response. *Adv. Funct. Mater.* **2011**, *21*, 756−763.
(23) Wu, Y. Z.; Zhu, W. H. Organic Sensitizers from D-π-A to D-A-π-A: Effect of the Internal Electron-Withdrawing Units on Molecular Absorption, Energy Levels and Photovoltaic Performances. *Chem. Soc. Rev.* **2013**, *42*, 2039−2058.
(24) Li, W. Q.; Wu, Y. Z.; Zhang, Q.; Tian, H.; Zhu, W. H. D-A-π-A Featured Sensitizers Bearing Phthalimide and Benzotriazole as Auxiliary Acceptor: Effect on Absorption and Charge Recombination Dynamics in Dye-Sensitized Solar Cells. *ACS Appl. Mater. Interfaces.* **2012**, *4*, 1822−1830.
(25) Chaurasia, S.; Hung, W. I.; Chou, H. H.; Lin, J. T. Incorporating a New 2*H*-[1,2,3]Triazolo[4,5-*c*]pyridine Moiety To Construct D−A−π−A Organic Sensitizers for High Performance Solar Cells. *Org. Lett.* **2014**, *16*, 3052−3055.
(26) Qin, C. J.; Islam, A.; Han, L. Y. Incorporating a Stable Fluorenone Unit into D−A−π−A Organic Dyes for Dye-Sensitized Solar Cells. *J. Mater. Chem.* **2012**, *22*, 19236−19243.
(27) Kang, X. W.; Zhang, J. X.; Rojas, A. J.; O'Neil, D.; Szymanski, P.; Marder, S. R.; El-Sayed, M. A. Deposition of Loosely Bound Organic D−A−π−A′ Dyes on Sensitized TiO_2 Film: a Possible Strategy to Suppress Charge Recombination and Enhance Power Conversion Efficiency in Dye-Sensitized Solar Cells. *J. Mater. Chem. A* **2014**, *2*, 11229−11234.
(28) Wang, L.; Shen, P.; Cao, Z. C.; Liu, X. P.; Huang, Y. S.; Liu, C. Y.; Chen, P.; Zhao, B.; Tan, S. T. Effects of the Acceptors in Triphenylamine-Based D−A−π−A′ Dyes on Photophysical, Electrochemical, and Photovoltaic Properties. *J. Power Sources* **2014**, *246*, 831−839.
(29) Ding, W. L.; Wang, D. M.; Geng, Z. Y.; Zhao, X. L.; Yan, Y. F. Molecular Engineering of Indoline-Based D−A−π−A Organic Sensitizers toward High Efficiency Performance from First-Principles Calculations. *J. Phys. Chem. C* **2013**, *117*, 17382−17398.
(30) Yang, J. B.; Ganesan, P.; Teuscher, J.; Moehl, T.; Kim, Y. J.; Yi, C. Y.; Comte, P.; Pei, K.; THolcombe, W.; Nazeeruddin, M. K.; Hua, J. L.; Zakeeruddin, S. M.; Tian, H.; Grätzel, M. Influence of the Donor Size in D−π−A Organic Dyes for Dye-Sensitized Solar Cells. *J. Am. Chem. Soc.* **2014**, *136*, 5722−5730.
(31) Li, Y. F. Molecular Design of Photovoltaic Materials for Polymer Solar Cells: Toward Suitable Electronic Energy Levels and Broad Absorption. *Acc. Chem. Res.* **2012**, *45*, 723−733.
(32) Ying, W. J.; Guo, F. L.; Li, J.; Zhang, Q.; Wu, W. J.; Tian, H.; Hua, J. L. Series of New D-A-π-A Organic Broadly Absorbing Sensitizers Containing Isoindigo Unit for Highly Efficient Dye-Sensitized Solar Cells. *ACS Appl. Mater. Interfaces* **2012**, *4*, 4215−4224.
(33) Shi, J.; Chen, J. N.; Chai, Z. F.; Wang, H.; Tang, R. L.; Fan, K.; Wu, M.; Han, H. W.; Qin, J. G.; Peng, T. Y.; Li, Q. Q.; Li, Z. High Performance Organic Sensitizers Based on 11,12-Bis(hexyloxy)-dibenzo[*a*,*c*]phenazine for Dye-Sensitized Solar Cells. *J. Mater. Chem.* **2012**, *22*, 18830−18838.
(34) Yang, X. C.; Zhao, J. H.; Wang, L.; Tian, J.; Sun, L. C. Phenothiazine Derivatives-Based D−π−A and D−A−π−A Organic Dyes for Dye-Sensitized Solar Cells. *RSC Adv.* **2014**, *4*, 24377−24383.
(35) Zeng, J.; Zhang, T. L.; Zang, X. F.; Kuang, D. B.; Meier, H.; Cao, D. R. D-A-π-A Organic Sensitizers Containing a Benzothiazole Moiety as an Additional Acceptor for Use in Solar Cells. *Sci. China Chem.* **2013**, *56*, 505−513.
(36) Seo, K. D.; Choi, I. T.; Park, Y. G.; Kang, S. W.; Lee, J. Y.; Kim, H. K. Novel D-A-π-A Coumarin Dyes Containing Low Band-Gap Chromophores for Dye-Sensitised Solar Cells. *Dyes Pigm.* **2012**, *94*, 469−474.
(37) Cui, Y.; Wu, Y. Z.; Lu, X. F.; Zhang, X.; Zhou, G.; Miapeh, F. B.; Zhu, W. H.; Wang, Z.-S. Incorporating Benzotriazole Moiety to Construct D-A-π-A Organic Sensitizers for Solar Cells: Significant Enhancement of Open-Circuit Photovoltage with Long Alkyl Group. *Chem. Mater.* **2011**, *23*, 4394−4401.
(38) Mao, J. Y.; Guo, F. L.; Ying, W. J.; Wu, W. J.; Li, J.; Hua, J. L. Benzotriazole-Bridged Sensitizers Containing a Furan Moiety for Dye-Sensitized Solar Cells with High Open-Circuit Voltage Performance. *Chem.—Asian J.* **2012**, *7*, 982−991.
(39) Yen, Y.-S.; Lee, C.-T.; Hsu, C.-Y.; Chou, H.-H.; Chen, Y.-C.; Lin, J. T. Benzotriazole-Containing D−π−A Conjugated Organic Dyes for Dye-Sensitized Solar Cells. *Chem.—Asian J.* **2013**, *8*, 809−816.
(40) Ying, L.; Hsu, B. B. Y.; Zhan, H.; Welch, G. C.; Zalar, P.; Perez, L. A.; Kramer, E. J.; Nguyen, T. Q.; Heeger, A. J.; Wong, W. Y.; Bazan, G. C. Regioregular Pyridal[2,1,3]thiadiazole π-Conjugated Copolymers. *J. Am. Chem. Soc.* **2011**, *133*, 18538−18541.
(41) Horie, M.; Kettle, J.; Yu, C.-Y.; Majewski, L. A.; Chang, S.-W.; Kirkpatrick, J.; Tuladhar, S. M.; Nelson, J.; Saunders, B. R.; Turner, M. L. Cyclopentadithiophene-Benzothiadiazole Oligomers and Polymers; Synthesis, Characterisation, Field-Effect Transistor and Photovoltaic Characteristics. *J. Mater. Chem.* **2012**, *22*, 381−389.
(42) Zhang, M.; Zhang, J.; Fan, Y.; Yang, L.; Wang, Y.; Li, R.; Wang, P. Judicious Selection of a Pinhole Defect Filler to Generally Enhance the Performance of Organic Dye-Sensitized Solar Cells. *Energy Environ. Sci.* **2013**, *6*, 2939−2943.
(43) Yan, P.; Xie, A.; Wei, M.; Loew, L. M. Amino(oligo)thiophene-Based Environmentally Sensitive Biomembrane Chromophores. *J. Org. Chem.* **2008**, *73*, 6587−6594.
(44) Gao, P.; Tsao, H. N.; Grätzel, M.; Nazeeruddin, M. K. Fine-Tuning the Electronic Structure of Organic Dyes for Dye-Sensitized Solar Cells. *Org. Lett.* **2012**, *14*, 4330−4333.
(45) Signh, P.; Baheti, A.; Thomas, K. R. J.; Lee, C.-P.; Ho, K.-C. Fluorene-Based Organic Dyes Containing Acetylene Linkage for Dye-Sensitized Solar Cells. *Dyes Pigm.* **2012**, *95*, 523−533.
(46) Frisch, M. J.; Trucks, G. W.; Schlegel, H. B.; Scuseria, G. E.; Robb, M. A.; Cheeseman, J. R.; Scalmani, G.; Barone, V.; Mennucci, B.; Petersson, G. A.; Nakatsuji, H.; Caricato, M.; Li, X.; Hratchian, H. P.; Izmaylov, A. F.; Bloino, J.; Zheng, G.; Sonnenberg, J. L.; Hada, M.; Ehara, M.; Toyota, K.; Fukuda, R.; Hasegawa, J.; Ishida, M.; Nakajima, T.; Honda, Y.; Kitao, O.; Nakai, H.; Vreven, T.; Montgomery, J. A.; Peralta, J. E.; Ogliaro, F.; Bearpark, M.; Heyd, J. J.; Brothers, E.; Kudin, K. N.; Staroverov, V. N.; Kobayashi, R.; Normand, J.; Raghavachari, K.; Rendell, A.; Burant, J. C.; Iyengar, S. S.; Tomasi, J.; Cossi, M.; Rega, N.; Millam, J. M.; Klene, M.; Knox, J. E.; Cross, J. B.; Bakken, V.; Adamo, C.; Jaramillo, J.; Gomperts, R.; Stratmann, R. E.; Yazyev, O.; Austin, A. J.; Cammi, R.; Pomelli, C.; Ochterski, J. W.; Martin, R. L.; Morokuma, K.; Zakrzewski, V. G.; Voth, G. A.; Salvador, P.; Dannenberg, J. J.; Dapprich, S.; Daniels, A. D.; Farkas, O.; Foresman, J. B.; Ortiz, J. V.; Cioslowski, J.; Fox, D. J. *Gaussian 09, Revision A.02*, Gaussian, Inc., Wallingford, CT, 2009.
(47) Becke, A. D. A New Mixing of Hartree−Fock and Local Density-Functional Theories. *J. Chem. Phys.* **1993**, *98*, 1372−1377.
(48) Pei, K.; Wu, Y. Z.; Islam, A.; Zhu, S. Q.; Han, L. Y.; Geng, Z. Y.; Zhu, W. H. Dye-Sensitized Solar Cells Based on Quinoxaline Dyes: Effect of π-Linker on Absorption, Energy Levels, and Photovoltaic Performances. *J. Phys. Chem. C* **2014**, *118*, 16552−16561.
(49) O'Regan, B.; Moser, J.; Anderson, M.; Grätzel, M. Vectorial Electron Injection into Transparent Semiconductor Membranes and Electric Field Effects on the Dynamics of Light-Induced Charge Separation. *J. Phys. Chem.* **1990**, *94*, 8720−8726.
(50) Barnes, P. R. F.; Liu, L. X.; Li, X. E.; Anderson, A. Y.; Kisserwan, H.; Ghaddar, T. H.; Durrant, J. R.; O'Regan, B. C. Re-evaluation of Recombination Losses in Dye-Sensitized Cells: The Failure of

Dynamic Relaxation Methods to Correctly Predict Diffusion Length in Nanoporous Photoelectrodes. *Nano Lett.* **2009**, *9*, 3532−3538.
(51) Barnes, P. R. F.; Anderson, A. Y.; Koops, S. E.; Durrant, J. R.; O'Regan, B. C. Electron Injection Efficiency and Diffusion Length in Dye-Sensitized Solar Cells Derived from Incident Photon Conversion Efficiency Measurements. *J. Phys. Chem. C* **2009**, *113*, 1126−1136.
(52) Gao, F.; Wang, Y.; Shi, D.; Zhang, J.; Wang, M. K.; Jing, X. Y.; Humphry-Baker, R.; Wang, P.; Zakeeruddin, S. M.; Grätzel, M. Enhance the Optical Absorptivity of Nanocrystalline TiO_2 Film with High Molar Extinction Coefficient Ruthenium Sensitizers for High Performance Dye-Sensitized Solar Cells. *J. Am. Chem. Soc.* **2008**, *130*, 10720−10728.
(53) Hamann, T. W.; Martinson, A. B. F.; Elam, J. W.; Pellin, M. J.; Hupp, J. T. Atomic Layer Deposition of TiO_2 on Aerogel Templates: New Photoanodes for Dye-Sensitized Solar Cells. *J. Phys. Chem. C* **2008**, *112*, 10303−10307.
(54) Usami, A.; Seki, S.; Mita, Y.; Kobayashi, H.; Miyashiro, H.; Terada, N. Temperature Dependence of Open-Circuit Voltage in Dye-Sensitized Solar Cells. *Sol. Energy Mater. Sol. Cells* **2009**, *93*, 840−842.
(55) Lu, M.; Liang, M.; Han, H.; Sun, Z.; Xue, S. Organic Dyes Incorporating Bis-hexapropyltruxeneamino Moiety for Efficient Dye-Sensitized Solar Cells. *J. Phys. Chem. C* **2011**, *115*, 274−281.
(56) Fabregat-Santiago, F.; Garcia-Belmonte, G.; Mora-Sero, I.; Bisquert, J. Characterization of Nanostructured Hybrid and Organic Solar Cells by Impedance Spectroscopy. *Phys. Chem. Chem. Phys.* **2011**, *13*, 9083−9118.
(57) Stergiopoulos, T.; Falaras, P. Minimizing Energy Losses in Dye-Sensitized Solar Cells Using Coordination Compounds as Alternative Redox Mediators Coupled with Appropriate Organic Dyes. *Adv. Energy Mater.* **2012**, *2*, 616−627.
(58) Luo, J.; Xu, M.; Li, R.; Huang, K.-W.; Jiang, C.; Qi, Q.; Zeng, W.; Zhang, J.; Chi, C.; Wang, P.; Wu, J. *N*-Annulated Perylene as an Efficient Electron Donor for Porphyrin-Based Dyes: Enhanced Light-Harvesting Ability and High-Efficiency Co(II/III)-Based Dye-Sensitized Solar Cells. *J. Am. Chem. Soc.* **2014**, *136*, 265−272.
(59) Li, L. L.; Chang, Y. C.; Wu, H. P.; Diau, E. W. G. Characterisation of Electron Transport and Charge Recombination Using Temporally Resolved and Frequency-Domain Techniques for Dye-Sensitised Solar Cells. *Int. Rev. Phys. Chem.* **2012**, *31*, 420−467.
(60) Liang, Y.; Peng, B.; Chen, J. Correlating Dye Adsorption Behavior with the Open-Circuit Voltage of Triphenylamine-Based Dye-Sensitized Solar Cells. *J. Phys. Chem. C* **2010**, *114*, 10992−10998.
(61) Fabregat-Santiago, F.; Bisquert, J.; Garcia-Belmonte, G.; Boschloo, G.; Hagfeldt, A. Influence of Electrolyte in Transport and Recombination in Dye-Sensitized Solar Cells Studied by Impedance Spectroscopy. *Sol. Energy Mater. Sol. Cells* **2005**, *87*, 117−131.
(62) Zong, X.; Liang, M.; Fan, C.; Tang, K.; Li, G.; Sun, Z.; Xue, S. Design of Truxene-Based Organic Dyes for High-Efficiency Dye-Sensitized Solar Cells Employing Cobalt Redox Shuttle. *J. Phys. Chem. C* **2012**, *116*, 11241−11250.
(63) Yang, X.; Zhang, K.; Liu, J.; Qin, C.; Chen, H.; Islama, A.; Han, L. Coordinated Shifts of Interfacial Energy Levels: Insight into Electron Injection in Highly Efficient Dye-Sensitized Solar Cells. *Energy Environ. Sci.* **2013**, *6*, 3637−3645.
(64) Li, S.-R.; Lee, C.-P.; Yang, P.-F.; Liao, C.-W.; Lee, M. M.; Su, W.-L.; Li, C.-T.; Lin, H.-W.; Ho, K.-C.; Sun, S.-S. Structure−Performance Correlations of Organic Dyes with an Electron-Deficient Diphenylquinoxaline Moiety for Dye-Sensitized Solar Cells. *Chem.—Eur. J.* **2014**, *20*, 10052−10064.